# TOPICS IN CONFINEMENT ANALYSIS OF TOKAMAKS WITH AUXILIARY HEATING

R.J. GOLDSTON

Princeton University
Plasma Physics Laboratory
Princeton, New Jersey 08544, USA

## Abstract

This lecture addresses a potpourri of topics in confinement analysis of tokamaks with auxiliary heating. First we discuss the different roles of on-line and off-line confinement analysis codes - what should the strengths of each be, and what are the allowable weaknesses? Next we examine the analysis of plasma rotation experiments, a topic which has not been formally treated in the literature. We discuss neutral beam injection of momentum into rotating plasmas, both in the context of Monte Carlo and of Fokker - Planck codes, taking into account time-changing 2-D plasma geometry. The transport equations for toroidal angular momentum, including the effects of momentum dissipation on power balance, are formulated.

Finally, we touch briefly on statistical techniques for interpreting confinement data bases. Simple models of the form: $\tau_E \propto I_p^a B_T^b \bar{n}_e^c \ldots$ are frought with danger. First of all, experience has shown that ohmic tokamak plasmas at low $\beta_p$ exhibit different scalings than strongly auxiliary-heated plasmas at high $\beta_p$. In addition, however, the results of simple multiple regression analyses can give misleading error bars for the coefficients a, b, c... above. If there is correlation in the data set amongst the "independent" variables $I_p$, $B_T$, $\bar{n}_e$... , then the uncertainty ranges of a, b, and c are correlated as well. This structure of the data is <u>not</u> reflected in the error bars generally considered. A simple way to study the joint confidence region of the fit coefficients, for situations with pairwise correlation of independent variables, is presented.

## I. On- and Off-Line Analysis Codes

Two major transport analysis codes are used on TFTR for interpreting confinement data. One code, TRANSP, which has been in development and in use at PPPL since 1978 (Ref. 1), does time and space-dependent analysis of current diffusion and energy and particle transport. It features a sophisticated Monte Carlo beam treatment, appropriate for careful calculations of beam-orbit effects, and of beam-related neutral collisions, which are important at high $P_b/\bar{n}_e$ (Ref. 2). TRANSP has recently been upgraded to treat time-changing $1^1/_2$ D plasma geometry, in order to handle TFTR compression and PBX beans. The second transport analysis code, SNAP, only performs time-independent analysis, and uses a relatively simple Fokker-Planck beam treatment. Its advantage is that it is quick to run, so that it can be used for between-shots data analysis during an experimental run. In addition, because SNAP requires much less data input than TRANSP, and therefore also much less data preparation, it is possible to prepare and maintain on disk hundreds, or even thousands of input data sets for SNAP, and then run literally hundreds of analyses in overnight batch jobs.

The natural mode of data analysis at TFTR is that shots are first analyzed with SNAP during the experimental runs. This helps the task force leader know whether the objectives of the run are being successfully met, while the run proceeds. Good shots are selected both during the run and after, and more careful data verification is performed. Large numbers of data sets are built up for each task force, and typically a substantial number of SNAP analyses are performed on each data set, using different assumptions for the more uncertain parameters (e.g. $\tau_p$ or $n_h/n_d$), and using different input data (e.g. neutron vs. X-ray crystal $T_i$, ECE vs. TVTS $T_e$). Because of the quantity of results generated in this manner, electronic database tools have become increasingly central to the process of studying SNAP transport analysis results.

Time-dependent transport analysis using the TRANSP code is limited to a much smaller set of discharges. These are typically selected for one of three reasons. First, the physics of interest may be intrinsically time-dependent, such as plasma compression or pellet injection. Second, the plasma conditions may be at the extremes of the data range where the more complete physics in TRANSP is needed to obtain acceptably accurate results. The energetic-ion mode in TFTR, where $n_b/n_e$ approaches 50%, and rotation speeds reach $6 \times 10^5$ m/sec is an example of such a regime. Finally, data sets which constitute the "premier" data, from which one intends to draw crucial

conclusions, are analyzed with TRANSP in order to be sure that no subtleties of importance have escaped the simpler code. TABLE 1 illustrates the different emphases of these two codes.

Table 1

| | SNAP | TRANSP |
|---|---|---|
| Magnetic geometry | Shifted circles | $1^1/_2$ D, multiple moments (Ref. 3) |
| Beam treatment | Simple Fokker-Planck (first orbit average) | Full Monte Carlo |
| Run time | 2 min. VAX 8600 | 20 hrs. VAX 8600 |
| Database interface | Online archives, easy electronic path from archives to databases | ≈1 MByte/TRANSP run; multiple runs stored on disk |

Clearly these two codes occupy different niches in the ecology of data interpretation. Interestingly, however, they are in some ways evolving towards one another. We are improving the SNAP beam treatment to include more of the beam-related atomic physics effects in TRANSP, such as beam-ion impact ionization of recycling neutrals. More general geometry will also be needed in SNAP as we move towards higher $\beta_p$ in TFTR. On the other hand, we will fit an arbitrary-geometry bounce-averaged Fokker-Planck treatment into TRANSP, to reduce CPU time for cases where detailed orbit physics is not required. Improved database interface tools for TRANSP will be developed as well. With these (and other) improvements to both codes, as well as continuing efforts to simplify data handling, we anticipate that their two ecological niches will remain separate, and that both species of code with evolve and flourish.

The TRANSP and SNAP codes have not yet been used to analyze plasma rotation experiments. This has previously been done at PPPL using standalone codes. Clearly there is a strong advantage to using the data-handling front end tools, and the database back end tools of these codes, for rotation studies. Furthermore as rotation speeds approach the plasma sound speed, the power flows associated with driving and damping toroidal rotation begin to play an important role in the overall power balance, and thus cannot be neglected in energy confinement analyses.

## II. Analysis of Plasma Rotation Data

### 1. Momentum Balance

Radial transport of toroidal angular momentum in tokamak plasmas is much more rapid than predicted on the basis of simple neoclassical theory. In neoclassical theory the transport of angular momentum is much slower than transport of energy or particles. This follows from the axisymmetry of the system, and the resulting intrinsic ambipolarity of neoclassical transport to rather high order in $\rho_\theta/a$. The fact that energy and momentum transport in experiments are roughly comparable provides a powerful clue into the mechanisms of transport in tokamaks. In order to analyze experimental data in detail, and in order to be able to compare the analyses from one experiment to another, it is important to formulate the momentum balance equations, including anomalous effects. With these equations in hand, we know precisely what we are speaking of when we compare "measured" momentum transport coefficients from one experiment to another. Furthermore, as plasma rotation speeds increase, we have to consider the power coupled into plasma rotation within the framework of the overall power balance equations we currently use.

We begin here by assuming for simplicity that all bulk ion species have the same $u_\phi$ and $T_i$ (which are assumptions others may choose to relax). We ignore the electrons for the purpose of studying momentum balance; for example fast ion momentum transferred collisionally to the electrons is assumed to be shared immediately with the ions. In a fixed, straight cylindrical system, the momentum conservation equation for the bulk plasma looks like:

$$\Sigma n_i m_i \frac{\partial u_\phi}{\partial t} + u_\phi \Sigma m_i \frac{\partial n_i}{\partial t} = F_{col} + F_{\mathbf{j}\times\mathbf{B}} + F_{bth} + F_{iz}$$
$$- \Sigma n_i m_i u_\phi \left[ \frac{1}{\tau_{\phi cx}} + \frac{1}{\tau_{\phi\delta}} \right] + \nabla\cdot(\Sigma n_i m_i)\chi_\phi \nabla u_\phi - \nabla\cdot \Sigma m_i \Gamma_i u_\phi \qquad \text{[eq. 1]}$$

Where the F's are collisional, $\mathbf{j}\times\mathbf{B}$, beam thermalization, and plasma ionization and recombination forces, described in more detail below. $\chi_\phi$ is the perpendicular momentum diffusivity which we are trying to deduce from

experimental data, so that it can be compared with theoretical calculations of anomalous transport or of more complex neoclassical effects (Ref. 4). $\tau_{\phi cx}$, $\tau_{\phi\delta}$ are local momentum loss times due to charge-exchange and field ripple. The field ripple may originate from the discrete nature of the toroidal field coil system or other machine asymmetries, or it can arise from plasma-induced magnetic perturbations, which couple to even axisymmetric machine structures (Ref. 5). Note that we have *assumed* here that particle convection carries momentum across flux surfaces.

For more general axisymmetric $1^1/_2$ D geometries we need to consider a toroidal system and angular momentum conservation, and so deal with torques, moments of inertia, and angular velocites, rather than forces, masses and velocities. Remember some definitions and results:

$$T \equiv \int R F \, d^3r$$

$$I \equiv \int \Sigma n m R^2 \, d^3r$$

$$P_\phi \equiv I\omega$$

$$I \frac{\partial \omega}{\partial t} = T - \omega \frac{\partial I}{\partial t} \qquad \text{[eq.'s 2]}$$

$$W_{rot} = \frac{\omega^2 I}{2}$$

$$\frac{\partial W_{rot}}{\partial t} = \omega T - \frac{\omega^2}{2} \frac{\partial I}{\partial t}$$

The final term in the last equation of this set is important, and will require clarification as we go along. A similar term appears in the energy balance for a straight cylinder.

In addition to working with angular momentum we would like to work with flux surface averages, and we would also like time-dependent geometry. If we assume $u_\phi \propto R$ on a flux surface (another assumption which others may choose to relax), then the appropriate flux surface quantity to deal with is $u_\phi/R$, or $\omega$, the angular velocity. The thermodynamic force driving momentum diffusion is then $\nabla\omega$, and the toroidal, flux surface averaged version of

equation 1 is:

$$\Sigma n_i m_i \langle R^2 \rangle \frac{\partial \omega}{\partial t} + \omega \langle R^2 \rangle \Sigma m_i \frac{\partial n_i}{\partial t} + \Sigma n_i m_i \omega \frac{\partial \langle R^2 \rangle}{\partial t}$$

$$+ \Sigma n_i m_i \langle R^2 \rangle \omega \left[\frac{\partial V}{\partial \rho}\right]^{-1} \frac{\partial}{\partial t} \frac{\partial V}{\partial \rho}$$

$$= T_{col} + T_{\mathbf{j}\times\mathbf{b}} + T_{bth} + T_{iz} - \Sigma n_i m_i \langle R^2 \rangle \omega \left[ \frac{1}{\tau_{\phi cx}} + \frac{1}{\tau_{\phi \delta}} \right]$$

$$+ \left[\frac{\partial V}{\partial \rho}\right]^{-1} \frac{\partial}{\partial \rho} \frac{\partial V}{\partial \rho} \Sigma n_i m_i \chi_\phi \langle R^2 (\nabla \rho)^2 \rangle \frac{\partial \omega}{\partial \rho}$$

$$- \left[\frac{\partial V}{\partial \rho}\right]^{-1} \frac{\partial}{\partial \rho} \frac{\partial V}{\partial \rho} \Sigma n_i m_i \omega \langle R^2 (\nabla \rho)^2 \rangle \left[\frac{\mathbf{v}_\rho}{\nabla \rho}\right] \qquad \text{[eq. 3]}$$

The terms on the left hand side represent the average angular momentum density stored in a flux surface. $\partial V/\partial \rho$ is a differential flux surface volume, where $\rho$ is an arbitrary flux surface label, which moves with the toroidal flux. $T_{col}$ is the collisional torque density. This can be calculated from a Monte Carlo sum of $n_b m_b R(B_\phi/B)(\partial v_{\|b}/\partial t)_{col}$. In the simplest drift equations where $|B| = |B_\phi|$ is assumed, the $(B_\phi/B)$ term is left out. One could imagine including higher order terms in $(\partial v_\phi/\partial t)$, but the fast ion drift equations itself is generally not solved including terms of higher order than the Alfvén drifts, so one would lose momentum conservation. Indeed it is important to use a drift formulation which conserves a canonical angular momentum (unlike the pure Alfvén drifts), and includes the presence of a radial electric field, as in Ref. 6. In simpler codes, a cylindrical Fokker-Planck solution can be performed in the rotating plasma frame, by transforming the beam velocity to the plasma frame. The collisional force can be derived in the manner of Ref. 7, (summing over all bulk plasma species). $T_{\mathbf{j}\times\mathbf{B}}$ is the average torque density exerted on the plasma due to any radial current of beam ions. This can be easily calculated via Monte Carlo; the change in mechanical angular momentum, $m_b R(B_\phi/B)v_{\|b}$, due to orbiting is taken to be delivered directly to the plasma. This topic has received theoretical attention in Ref. 8. In quasi-cylindrical codes it would be appropriate to give the difference between the input neutral beam momentum and the first-orbit-averaged momentum (including radial electric fields and banana precession) to the plasma as $T_{\mathbf{j}\times\mathbf{B}}$. The initial pitch angle in a cylindrical formulation would

then be chosen such that the first-orbit- averaged momentum was delivered to the Fokker-Planck equation. $T_{bth}$ is the torque delivered to the plasma in the form of thermalized beam ions with finite lab-frame toroidal velocity. This is easily calculated via Monte Carlo, and can be derived from the slowing down rate and from the first two Legendre harmonics of the distribution function in the lowest energy zone of a Fokker-Planck solution. (We return to the topic of beam-ion slowing down in section 2B.) $T_{iz}$ is the torque density due to ionizing new rotating neutrals into the ion distribution function and losing rotating ions via recombination. Loss from the ion distribution function via charge-exchange with beam neutrals should be included here as well.

$\tau_{\phi cx}$ is the momentum loss time to charge-exchange. One has to recognize that neutral atoms may be rotating at a speed close to that of the bulk plasma, so that the charge-exchange part of this term is not just the charge-exchange time. To fair accuracy $\tau_{\phi cx} \approx \tau_{cx}[u_\phi/(u_\phi - u_{\phi o})]$. To do this properly, one should include toroidal rotation in the neutral transport codes, and calculate $u_{\phi o}$ (or better yet, $\tau_{\phi cx}$) directly. For the time being we can perhaps assume $u_\phi/(u_\phi - u_{\phi o}) \approx T_i/(T_i - T_o)$.

The term including $\chi_\phi$ reflects momentum diffusion, or perpendicular viscosity, in units of $l^2/t$. This particular formulation comes from assuming that the cross-field flux of angular momentum ($\Gamma_\phi$) driven by $\nabla\omega$ is given by:

$$\Gamma_\phi = \Sigma n_i m_i \chi_\phi R^2 \nabla\rho \frac{\partial\omega}{\partial\rho} \qquad \text{[eq. 4]}$$

and so

$$\int \Gamma_\phi \cdot d\mathbf{A} = \Sigma n_i m_i \chi_\phi (2\pi \oint dl_p |\nabla\rho| R^3) \frac{\partial\omega}{\partial\rho} \qquad \text{[eq. 5]}$$

Since the definition of the flux surface average of any quantity X is:

$$\langle X \rangle \equiv [2\pi \oint dl_p (XR/|\nabla\rho|)] \left[\frac{\partial V}{\partial\rho}\right]^{-1} \qquad \text{[eq. 6]}$$

we have:

$$\int \Gamma_\phi \cdot d\mathbf{A} = \left\{\frac{\partial V}{\partial\rho}\right\} \Sigma n_i m_i \chi_\phi \langle R^2 (\nabla\rho)^2 \rangle \frac{\partial\omega}{\partial\rho} \qquad \text{[eq. 7]}$$

The $\chi_\phi$ term of equation 3 follows by conservation of angular momentum.

The last term in equation 3 represents convection of momentum across flux surfaces. Here we are taking what one might call the "average Joe" model of convection, *assuming* that the convected particles carry the average

local angular momentum with them. Other weightings could be treated as off-diagonal elements in the matrix of transport coefficients. The particular form for the convection of momentum in eq. 3 follows from the same sort of arguments as eq.'s 4 - 7, if we assume that $\Gamma_i \propto \nabla p$ along a flux surface, as we have assumed for $\Gamma_\phi$. Note that in transport analysis codes $D_i$ is deduced from measured fluxes, rather than the other way around as in simulation codes.

## 2. Energy Balance associated with Rotation

### A. Source-Friction

It is important to follow all of the energy flows implied by equations 1 and 3, so that we can make up a proper energy balance for the beam ions, the plasma thermal energy, and the plasma rotational energy. First, however, it is instructive to look at power balance in a very simple problem, in which a moving plasma with velocity $\mathbf{u}_{rot}$ and temperature T has a source rate of ions S moving at velocity $\mathbf{u}_S$, for example due to electron ionization of neutrals. In this case we have the obvious equations:

$$\frac{dn}{dt} = S \qquad \text{Particle Conservation} \qquad \text{[eq. 8]}$$

$$\frac{d}{dt}(nm\mathbf{u}_{rot}) = Sm\mathbf{u}_S \qquad \text{Momentum Conservation} \qquad \text{[eq. 9]}$$

$$\frac{d}{dt}\left[\frac{nm\mathbf{u}_{rot}^2}{2} + \frac{3nkT}{2}\right] = Sm\mathbf{u}_S^2/2$$

$$\text{Energy Conservation} \qquad \text{[eq. 10]}$$

Substituting equation 8 into equation 9 we get

$$nm\frac{d}{dt}\mathbf{u}_{rot} = Sm(\mathbf{u}_S - \mathbf{u}_{rot}) \qquad \text{[eq. 11]}$$

which is not surprising. However, substituting equations 8 and 11 into equation 10 we get

$$\frac{d}{dt}\frac{3nkT}{2} = \frac{Sm(\mathbf{u}_{rot} - \mathbf{u}_S)^2}{2} \qquad \text{[eq. 12]}$$

Equation 12 simply shows that the net particle energy in the plasma frame goes into increasing plasma thermal energy. This is what we generally label as $P_{bth}$.

It is now instructive to think about this case by constructing an energy balance equation from the momentum balance equation. The R.H.S. of equation 9 can be viewed as a force, $\mathbf{F}_S$, giving rise to a time rate of change of momentum. Multiplying both sides by $\mathbf{u}_{rot}$ and substituting equation 8 gives

$$\frac{d}{dt}\frac{nm\mathbf{u}_{rot}^2}{2} = \mathbf{F}_S\cdot\mathbf{u}_{rot} - \frac{Sm\mathbf{u}_{rot}^2}{2} \qquad \text{[eq. 13]}$$

Note, then, that the energy in plasma motion is increased by a work-like term of the form $\mathbf{F}_S\cdot\mathbf{u}_{rot}$, and decreased by a new term which we might call source-friction. This is the linear momentum analog of the last term in the last equation of equations 2. Note that the $\mathbf{F}_S\cdot\mathbf{u}_{rot}$ term here is quite different from the input power associated with the new ions even if $\mathbf{u}_S = \mathbf{u}_{rot}$. However when we add up the R.H.S.'s of equations 12 and 13 we do, of course, obtain the original input power, $Sm\mathbf{u}_S^2/2$. In the special case where $\mathbf{u}_S = \mathbf{u}_{rot}$, the two terms in equation 13 sum to the input power and the $P_{bth}$ thermalization power is, of course, zero.

B. Beam ion slowing down

The excercise we have just completed will allow us to better understand the relationship of the rotational power balance to the thermal power balance. In particular it addressed issues which will be important in understanding effects associated with beam ions and plasma neutrals being delivered to a rotating bulk ion distribution. We have not completed the discussion, however, of how to obtain energy balance in the calculation of beam ion slowing down in a rotating plasma. In Monte Carlo codes beam ion orbits are followed in the lab frame, so at each collisional time step the beam ion velocity must be transformed to the local rest frame of the plasma. Since the drift velocities (including **ExB** drifts) are ordered small, we need only include the parallel component of $u_\phi$ in the transformation [$\Delta v_{\|b} = -(B_\phi/B)u_\phi$]. Collisions can then be executed with the usual Monte Carlo techniques. (For simplified drift equations with $|B| = |B_\phi|$ we take $\Delta v_{\|b} = -u_\phi$ .) The loss of plasma-frame energy from collisions simply goes into plasma heating as before. In the lab frame a different amount of energy

is lost, however. Taking the plasma-frame beam ion velocity to be

$$\mathbf{v}_{pl} \equiv \mathbf{v}_{lab} - \mathbf{u}_{\|rot} \qquad \text{[eq. 14]}$$

we can evaluate the time derivative of the lab-frame energy due to collisions:

$$\left.\frac{d}{dt}\right|_{col} \frac{m_b v^2_{lab}}{2} = \left.\frac{d}{dt}\right|_{col} \frac{m_b v^2_{pl}}{2} + m_b \mathbf{u}_{\|rot} \cdot \left.\frac{d}{dt}\right|_{col} \mathbf{v}_{lab} \qquad \text{[eq. 15]}$$

where we have used $(d/dt)_{col}\mathbf{v}_{lab} = (d/dt)_{col}\mathbf{v}_{pl}$. Thus the extra lab-frame energy loss goes into simple $\mathbf{F}_{col} \cdot \mathbf{u}_{rot}$. Any net perpendicular $\mathbf{F}_{col}$ due to the beam ions is neglected. There is also a beam-driven torque due to $\mathbf{j}_b \times \mathbf{B}_p$, which corresponds to the change in mechanical angular momentum of beam ions as they cross flux surfaces. It can be shown from conservation of canonical angular momentum that the $\omega T_{\mathbf{j}\times\mathbf{B}}$ power which results from this force is exactly balanced by the radial motion of beam ions up or down the electrostatic potential.

In section 1 we discussed how simple Fokker-Planck calculations can be performed in a rotating plasma, by transforming the beam ion velocities to the plasma frame when the beam ions are first deposited, and then performing the usual flux-surface-local slowing down calculations. (We also discussed how to take into account the first-orbit $\mathbf{j}_b \times \mathbf{B}_p$ torque.) The approach we outlined is a bit curious, since it leads one to wonder about what becomes of the energy difference between $m_b v_{lab}^2/2$ and $m_b v_{pl}^2/2$. However, we note that we can simply time-integrate equation 15, and find

$$\left.\frac{1}{2} m_b v^2_{lab}\right|_0^t = \left.\frac{1}{2} m_b v^2_{pl}\right|_0^t + \left. m_b \mathbf{u}_{\|rot} \cdot (\mathbf{v}_{lab})\right|_0^t . \qquad \text{[eq.16]}$$

Thus again the lab-frame energy goes directly into plasma heating, and into $\mathbf{F}\cdot\mathbf{u}$ power. Note that for strict energy accountability, beam ion charge exchange losses will need to be transformed back into the lab frame. The power density of charge-exchange loss in the plasma frame is given by

$$Q_{cx} = \int f_b E_{b,pl} \upsilon_{cx} d\xi_{pl} 2\pi v_{pl}^2 dv_{pl} \qquad \text{[eq. 17]}$$

where $\xi_{pl} \equiv v_{\parallel,pl}/v_{pl}$, and $f_b$ can be conveniently expressed in Legendre polynomials. To find the energy loss in the lab frame, we need only replace $E_{b,pl}$ ($\equiv m_b v_{pl}^2/2$) with $E_{b,lab}$ using

$$E_{b,lab} = \frac{m_b}{2}\left[(u_\parallel + v_{pl}\xi_{pl})^2 + (1-\xi_{pl}^2)v_{pl}^2\right]$$
$$= E_{b,pl} + \frac{m_b}{2}(u_\parallel^2 + 2u_\parallel v_{pl}\xi_{pl}) \qquad \text{[eq. 18]}$$

The integral $d\xi_{pl}$ of eq. 17, using $E_{b,lab}$, will only include the first two Legendre polynomials. Note that in this formulation we have ignored the difference between $u_\parallel$ and $u_\phi$, and between $v_\parallel$ and $v_\phi$, assuming that the momentum input to the Fokker-Planck calculation was $Smv_\parallel$.

In a Fokker-Planck calculation, the thermalization force, $F_{bth}$, can be found by integrating the flow of momentum across the lowest energy zone. This is similar to the problem of calculating the plasma-frame charge-exchange loss. The general form of the slowing down equation is

$$\frac{\partial f_b}{\partial t} = -\frac{1}{v^2}\frac{\partial}{\partial v}v^2\left.\frac{\partial v}{\partial t}\right|_{col} f_b + \text{C.X. terms}$$
$$+ \text{Pitch-angle scattering terms.} \qquad \text{[eq. 19]}$$

Integrating by parts we get that the flow of momentum to thermalization per unit volume is

$$\left.\frac{\partial P_\phi}{\partial t}\right|_{th} = -\int f_b(v=v_{th})p_\phi 2\pi d\xi_{pl} v_{th}^2 \left.\frac{\partial v}{\partial t}\right|_{col,\ v=vth} \qquad \text{[eq. 20]}$$

$p_\phi$ in the lab frame for this case is $m_b(v_{th}\xi_{pl} + u_\parallel)$. Thus we see again that only the first 2 Legendre harmonics will be needed.

In the general geometry, Monte Carlo case we will take the thermalization torque, $T_{bth}$, to be $\Sigma m_b v_{b,\parallel}(B_\phi/B)R_s$, where $R_s$ is the major radius at which the fast ions are thermalized, and $v_{b,\parallel}$ the beam ion toroidal velocity. In this case there is a new effect because $R_s^2 \neq \langle R^2\rangle$. Another way to say this is that the $(\omega^2/2)\partial I/\partial t$ term of equations 2 associated with beam ion thermalization is represented in general geometry by the beam part of $(\omega^2/2)\Sigma m_i(\partial V/\partial\rho)^{-1}\langle R^2\rangle\partial/\partial t(n_i\partial V/\partial\rho)$. However in the beam ion power balance this equation has $R_s^2$, rather than $\langle R^2\rangle$, by analogy with equation 13. This paradox is resolved by realizing that beam ions thermalized unevenly across the flux surface will exchange bulk rotational energy for thermal

energy as they spread out. In particular, if they are deposited towards the inside in major radius they will take energy out of rotation as they distribute outwards, and vice-versa for ions deposited outboard in major radius. The net effect is a new term in $P_{bth}$

$$\Delta P_{bth} = \frac{\omega^2}{2} m_b(\langle R^2\rangle\langle S_{i,bth}\rangle - \langle R_s^2 S_{i,bth}\rangle) \qquad \text{[eq. 21]}$$

This new term does remind us of the fact that our assumption that $n_i = n_i(\rho)$ only, rests on shaky ground at high rotation speeds. Another uncertain assumption is that the beam ion source rate due to thermalization is the only ion source rate with poloidal variation.

C. Power Balance

It is interesting to generate a power balance equation in the spirit of equation 13, based on the fixed, cylindrical model equation 1. Multiplying both sides by $u_\phi$, we obtain

$$\Sigma n_i m_i \frac{1}{2}\frac{\partial u_\phi^2}{\partial t} + \frac{1}{2} u_\phi^2 \Sigma m_i \frac{\partial n_i}{\partial t} =$$

$$- \frac{1}{2} u_\phi^2 \Sigma m_i \frac{\partial n_i}{\partial t} + u_\phi F_{col} + u_\phi F_{jxb} + u_\phi F_{bth} + u_\phi F_{iz}$$

$$- \Sigma n_i m_i u_\phi^2 \left[ \frac{1}{\tau_{\phi cx}} + \frac{1}{\tau_{\phi\delta}} \right]$$

$$+ u_\phi \nabla\cdot(\Sigma n_i m_i)\, \chi_\phi \nabla u_\phi - u_\phi \nabla\cdot \Sigma m_i \Gamma_i u_\phi \qquad \text{[eq. 22]}$$

I have placed the time derivative of the stored rotational energy density on the L.H.S.. The first terms on the right hand side can be identified as the source-friction, plus four $\mathbf{F}\cdot\mathbf{u}_{rot}$ work terms. Remember, however, that the $u_\phi F_{bth}$ term contains twice the rotational energy associated with the plasma-frame isotropic part of the thermalizing beam ions. If we add the negative source-friction term associated with the beam-driven $dn_i/dt$, we then have the correct beam energy balance. The loss rate of rotational energy via $\tau_{\phi cx}$ and $\tau_{\phi\delta}$ is twice the rate of loss of momentum, which is the

expected result for charge exchange with slower-moving thermal neutrals or ripple drag. In the case of recombination, or charge exchange loss via collisions with beam neutrals, where net momentum is changed by changing the total number of particles, one expects half this rate. $u_\phi F_{iz}$ plus the negative ion source rates associated with these processes acting through the source-friction term, give the proper net effect on rotational energy. The meaning of equation 22 becomes clearer if we substitue $\partial n_i/\partial t = -\nabla\cdot\Gamma_i + S_{i,bth} + S_{iz}$, and volume integrate from 0 to r.

$$4\pi^2 R_0 \int \left[ \Sigma n_i m_i \frac{1}{2}\frac{\partial u_\phi^2}{\partial t} + \frac{1}{2} u_\phi^2 \Sigma m_i \frac{\partial n_i}{\partial t} \right] r dr =$$

$$4\pi^2 R_0 \int \Big[ u_\phi F_{col} + u_\phi F_{jxb} - \frac{1}{2} u_\phi^2 \Sigma m_i (S_{i,bth} + S_{iz}) + u_\phi F_{bth}$$

$$+ u_\phi F_{iz} - \Sigma n_i m_i u_\phi^2 \left[ \frac{1}{\tau_{\phi cx}} + \frac{1}{\tau_{\phi\delta}} \right] \Big] \, r dr$$

$$- 4\pi^2 R_0 \int (\Sigma n_i m_i) \chi_\phi (\nabla u_\phi)^2 r dr + 4\pi^2 R_0 r u_\phi (\Sigma n_i m_i) \chi_\phi \frac{\partial u_\phi}{\partial r}$$

$$- 2\pi^2 R_0 r \Sigma m_i (\Gamma_i \cdot \hat{\mathbf{r}}) u_\phi^2$$

[eq. 23]

This equation makes clear the distinction between local dissipation of rotational energy into heat, and radial transport of rotational energy. New local heating terms are thus introduced into (presumably) the ion energy balance equation:

$$\frac{3}{2}\frac{\partial}{\partial t}\Sigma n_i T_i = (\text{previous terms})^* + \frac{\Sigma n_i m_i u_\phi^2}{\tau_{\phi\delta}} + \Sigma n_i m_i \chi_\phi (\nabla u_\phi)^2$$

[eq. 24]

*See equation 31

The last step in this power balance problem is to create an arbitrary geometry generalization of equation 22, by multiplying equation 3 by $\omega$, in the spirit of equations 2.

$$\Sigma n_i m_i \frac{1}{2}\langle R^2\rangle \frac{\partial \omega^2}{\partial t} + \frac{1}{2}\omega^2\langle R^2\rangle \Sigma m_i \frac{\partial n_i}{\partial t}$$

$$+ \frac{1}{2}\Sigma n_i m_i \omega^2 \frac{\partial \langle R^2\rangle}{\partial t}$$

$$+ \frac{1}{2}\Sigma n_i m_i \langle R^2\rangle \omega^2 \left[\frac{\partial V}{\partial \rho}\right]^{-1} \frac{\partial}{\partial t}\frac{\partial V}{\partial \rho}$$

$$= -\frac{1}{2}\Sigma n_i m_i \omega^2 \frac{\partial \langle R^2\rangle}{\partial t}$$

$$-\frac{1}{2}\omega^2 \Sigma m_i \langle R^2\rangle \left[\frac{\partial V}{\partial \rho}\right]^{-1} \frac{\partial}{\partial t} n_i \left[\frac{\partial V}{\partial \rho}\right]$$

$$+ \omega T_{col} + \omega T_{jxb} + \omega T_{bth} + \omega T_{iz}$$

$$- \Sigma n_i m_i \langle R^2\rangle \omega^2 \left[\frac{1}{\tau_{\phi cx}} + \frac{1}{\tau_{\phi \delta}}\right]$$

$$+ \omega\left[\frac{\partial V}{\partial \rho}\right]^{-1} \frac{\partial}{\partial \rho}\frac{\partial V}{\partial \rho} \Sigma n_i m_i \chi_\phi \langle R^2(\nabla \rho)^2\rangle \frac{\partial \omega}{\partial \rho}$$

$$- \omega\left[\frac{\partial V}{\partial \rho}\right]^{-1} \frac{\partial}{\partial \rho}\frac{\partial V}{\partial \rho} \Sigma n_i m_i \omega \langle R^2(\nabla \rho)^2\rangle \left[\frac{\mathbf{v}_\rho}{\nabla \rho}\right] \qquad \text{[eq. 25]}$$

All of the terms in this equation are simply identified with the terms in equation 22, except for the first term on the R.H.S., which takes account of compression effects. It reflects the fact that the rotational energy per particle is proportional to $1/R^2$. Integrating eq. 25 over volume clearly gives rise to an analog of equation 23. The generalized geometry version of equation 24 becomes:

$$\frac{3}{2}\frac{\partial}{\partial t}\Sigma n_i T_i = (\text{previous terms})^* + \frac{\Sigma n_i m_i \langle R^2\rangle \omega^2}{\tau_{\phi \delta}}$$

$$+ \frac{\omega^2}{2} \dot{m}_b(\langle R^2\rangle\langle S_{i,bth}\rangle - \langle R_s^2 S_{i,bth}\rangle) \qquad ^*\text{See equation 31}$$

$$+ \Sigma n_i m_i \chi_\phi \langle R^2(\nabla \rho)^2\rangle \left[\frac{\partial \omega}{\partial \rho}\right]^2$$

$$+ \frac{\Sigma n_i m_i}{2}\left[\frac{\mathbf{v}_\rho}{\nabla \rho}\right]\left[\langle(\nabla \rho)^2\rangle \frac{\partial}{\partial \rho}\omega^2\langle R^2\rangle - \langle R^2(\nabla \rho)^2\rangle \frac{\partial \omega^2}{\partial \rho}\right] \qquad \text{[eq. 26]}$$

The last term does not exist in a cylinder; it arises from the same physics as the $S_{i,bth}$ term, given the assumption of $\mathbf{v}_p \propto \nabla p$.

3. Ancillary Effects

A. Beam Deposition

It is necessary to take into account the fact that the plasma is rotating, in the atomic physics calculations. This is straightforward in the sense that one need only make a vector subtraction of the beam and plasma velocities to get a new relative velocity between the two, and then proceed to calculate reaction rates with this new $v_{rel}$, as before.

B. Charge-Exchange Analysis

This is really the same thing as for beam deposition, except we also need to launch the neutrals from a shifted Maxwellian, although one could question this approximation for $f_i$.

C. Beam/plasma $\beta$'s

The beam $\beta$ calculation in Monte Carlo codes is unchanged; $w_{\parallel,b}$ and $w_{\perp,b}$ are accumulated in the lab frame via Monte Carlo techniques as before. In Fokker-Planck codes, however, the beam distribution function is calculated in the plasma frame. $w_{\perp,b}$ can be calculated as before, but $w_{\parallel,b}$ must be evaluated in the lab frame, using equation 18.

Stored energy in rotation looks to magnetic measurements just like stored energy in $w_{\parallel,b} = (1/2)mv_{b\parallel}^2$, to first order in inverse aspect ratio. Thus $\beta_\parallel$ due to rotation is simply $2\langle U_{rot}\rangle/(B^2/8\pi)$, where $\langle U_{rot}\rangle$ is the volume-average energy density in rotation. There is no effect on $\beta_\perp$. $\beta^{eq}$ (the quantity measured via the vertical field strength required for equilibrium) is given, as always, by $\beta^{eq} = (\beta_\parallel + \beta_\perp)/2$. At high rotation speeds the plasma anisotropy will need to be included in MHD equilibrium calculations for transport analysis.

D. Neutral transport

It should be relatively straightforward to generalize current Monte Carlo neutral transport codes to include a rotating background plasma. The

necessary physics for power balance is described in section 2A, since the Monte Carlo neutrals represent δ-function distributions of particles, which is what is treated there. Note the particular definition of power to the thermal plasma due to ionization; the same term with a negative sign will occur for loss of particles from the ion distribution.

For a model where one considers the neutrals as a rotating fluid, the discussion in section 2A needs to be expanded. The clearest way to do this is to consider two groups of particles, neutrals with mean velocity $\mathbf{u}_0$ and average thermal temperature around this velocity $T_0$, and ions with mean velocity $\mathbf{u}_i$ and thermal spread $T_i$. Define $S_{0i}$ to be the source rate of ions from the neutrals, and $S_{i0}$ to represent the reverse process. Then we proceed in parallel with the discussion in 2A.

$$\frac{dn_i}{dt} = -\frac{dn_0}{dt} = S_{0i} - S_{i0}$$

Particle Conservation [eq. 27]

$$\frac{d}{dt}(n_i m_i \mathbf{u}_i) = -\frac{d}{dt}(n_0 m_i \mathbf{u}_0) = S_{0i} m_i \mathbf{u}_0 - S_{i0} m_i \mathbf{u}_i$$

Momentum Conservation [eq. 28]

$$\frac{d}{dt}\left[\frac{n_i m_i \mathbf{u}_i^2}{2} + \frac{3}{2} n_i k T_i\right] = -\frac{d}{dt}\left[\frac{n_0 m_0 \mathbf{u}_0^2}{2} + \frac{3}{2} n_0 k T_0\right] =$$

$$S_{0i}\left[\frac{m_i \mathbf{u}_0^2}{2} + \frac{3}{2} k T_0\right] - S_{i0}\left[\frac{m_i \mathbf{u}_i^2}{2} + \frac{3}{2} k T_i\right]$$

Energy Conservation [eq. 29]

Substituting equation 27 into equation 28 we get

$$n_i m_i \frac{d}{dt} \mathbf{u}_i = S_{0i} m_i (\mathbf{u}_0 - \mathbf{u}_i) \qquad \text{[eq. 30]}$$

which is not surprising. However, substituting equations 27 and 30 into equation 29 we get

$$\frac{d}{dt}\frac{3}{2} n_i k T_i = \frac{3}{2} S_{0i} k T_0 - \frac{3}{2} S_{i0} k T_i + \frac{1}{2} S_{0i} m_i (\mathbf{u}_i - \mathbf{u}_0)^2$$

[eq. 31]

The first term represents the familiar charge-exchange and ionization power, expressed in the simplest way. The third term is new, and so somewhat gives the lie to the "previous terms" entry in equations 24 and 26. In effect the familiar $P_{cx}$ and $P_{iz}$ terms in the ion power balance have new parts. These can be understood very simply. Suppose we have cool neutral and ion fluids, moving in opposite directions at substantial velocity. If we let these two fluids charge exchange with each other for a long time, eventually they will come to rest, and their directed energy will have been converted to thermal motion. The same argument holds if one distribution is simply ionized into the other.

E. Poloidal Variation of $n_i$

In all of this analysis we have assumed $n_i$ was a flux-surface constant. This is tantamount to assuming $2\epsilon u_\phi^2 << v_{th}^2$, which is clearly not true for impurity ions under recent conditions in TFTR. It also assumes that there is no significant poloidal variation of the beam ion density - clearly incorrect for high-power perpendicular injection. It would be valuable to at least calculate the theoretical $n_i(\theta)$ for each species. A simple calculation is available in Ref. 9.

F. Beam-driven Current

The beam-driven current is as easily calculated in a rotating plasma as in a stationary one. The calculation must simply be done in the plasma frame. Corrections for the difference between the net current and the raw rotating beam ion current ($1-1/Z_{eff}$ for classical, plus trapping corrections for neo-classical) must be taken into account. A recent investigation (Ref. 10) indicates that the usual calculation of the combined effect of the toroidal electric field and the distortion of the electron distribution function on the beam ions, the so-called $E_\parallel^*$ term (Ref. 11), neglects a part of the distorion of $f_e$ which becomes important (relative to $E_\parallel^*$) when the raw circulating beam ion current becomes comparable to the total plasma current. In a classical plasma the term results in a reduction in the electron drag by

$$\left.\frac{\partial v_\parallel}{\partial t}\right|_e = \frac{n_b \langle v_{b\parallel,pl} \rangle}{n_e Z_{eff} \tau_s} \qquad \text{[eq. 32]}$$

## III. Statistical Techniques for Interpreting Confinement Results

As the quantity of data available from diagnostics and from data interpretation codes has grown, our dependence on electronic database tools has increased as well. The flexible and powerful LOCUS system (Ref. 12) developed at PPPL has proven to be a tremendously valuable tool in the day-to-day work of essentially all of the TFTR physicists. This has the fortunate consequence that we are able to handle a very large quantity of data in the traditional ways. In the simplest sense, we are able to just plot more points on paper, without spending proportionately more time doing it. On a more subtle level, these tools allow us to do more kinds of investigations - examine data from many different viewpoints in order to see what can be learned. Database tools can be used to compare massive quantities of experimental results with theoretical prediction, and look for trends in the patterns of agreement and disagreement. On the other hand, they can also be used in the data verification process to look for inconsistencies or odd behavior in the data. The ability to plot data easily in many different ways, however, does not obviate the need for careful planning of experiments and careful scrutiny of analysis procedures.

Increased quantities of data, stored electronically, have naturally led to increased use of statistical tools. Again here we find a realm of great power and flexibility, but considerable danger. There is a strong tendency to rely on multiple regression analysis to do data interpretation, in some sense, for us. A clear example of how this can be misleading comes from the fact that we know that simple models of the form $\tau_E \propto I_p^a B_T^b \bar{n}_e^c$ cannot adequately represent all tokamak confinement data. Density and current scans in low $\beta_p$ ohmic discharges give very different results than scans of the same parameters in high $\beta_p$ beam-heated plasmas. In particular, if $\tau_E \propto \bar{n}_e^1$ is observed in ohmic data, and $\tau_E \propto \bar{n}_e^0$ in high-power beam-heated plasmas, there is no way that the constraints imposed by ohmic heating can be "relaxed" in a way that allows the same scaling law to explain both regimes. However statistical fits to data which include both categories of plasmas, perhaps without the lowest-density ohmic cases, or the highest-power beam cases, will give reasonably good-looking regression plots. How many of us study residuals from the fits we make, to look for patterns in the errors, and therefore inadequacy of the models? Even this is not a substitute for carefully controlled experiments with systematic scans of individual parameters, covering as much of parameter space as possible.

Another pitfall of multiple linear regression comes from the presence of correlation between nominally independent variables. In ohmic data, for example, there tends to be a correlation of $I_p$ and $\bar{n}_e$. If there is such correlation, one consequence is that the error bars in the fit parameters for $I_p$ and $\bar{n}_e$ are not independent. If the fit parameter for $I_p$ is chosen near the top of its error range, then the fit parameter for $\bar{n}_e$ must be taken near the bottom of its range. For a concrete example, we will consider plasma rotation measurements on PDX, reported in the doctoral thesis of Kevin Brau (Ref. 13). See Fig. 1 below. In this figure $v_{phi}$ represents the central toroidal rotation speed, measured by X-ray crystal spectroscopy (Ref. 14); $P_{abs}$ is the absorbed beam power. Note that there is a strong correlation of the line average density with the injected beam power. This will make it difficult to disentangle dependencies on density and power. (In addition there is a correlation with $I_p$ in this data, which we will not discuss here.)

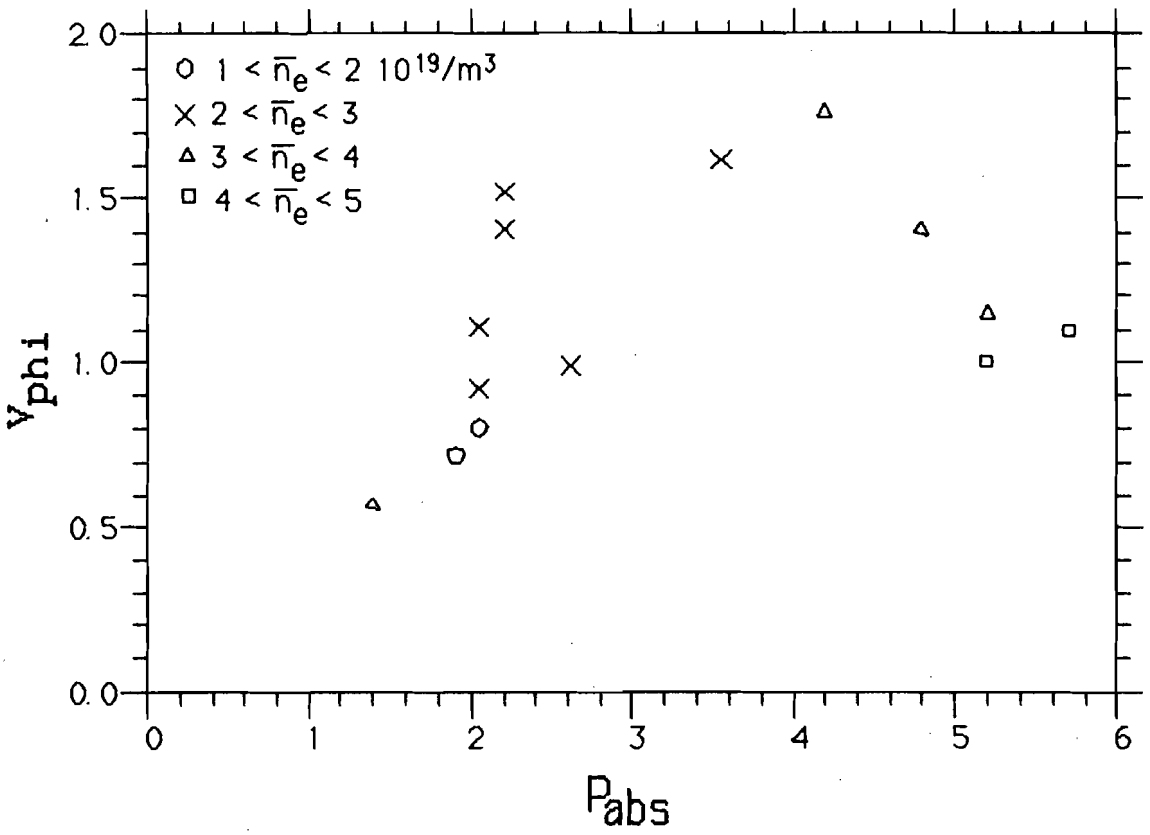


**Figure 1.** Toroidal rotation speed vs. absorbed beam power from PDX.

Data from PLT suggested that $v_\phi$ was proportional to $P_{abs}$ and nearly independent of $\bar{n}_e$. Looking at the saturation of rotation speed with

increasing $P_{abs}$ in this figure certainly suggests that the PDX data is quite different. But how do we prove this statistically? If we model $v_\phi \propto P_{abs}^{\alpha} \bar{n}_e^{\beta}$ regression analysis gives individual 90% confidence ranges for $\alpha$ and $\beta$ of $0.23 < \alpha < 1.04$, and $-1.28 < \beta < 0$, so this would *seem* to indicate that $P_{abs}^{1}\bar{n}_e^{0}$ cannot be excluded. However we really need to study the joint confidence range of $\alpha$ and $\beta$ together, since there is significant correlation of $P_{abs}$ and $\bar{n}_e$ in the data set.

Graduate statistics texts (Ref. 15) give a simple formula defining the joint confidence region by:

$$\frac{(\boldsymbol{\beta}-\hat{\boldsymbol{\beta}})'\mathbf{X}'\mathbf{X}(\boldsymbol{\beta}-\hat{\boldsymbol{\beta}})}{pMS_E} \leq F_{\alpha,p,n-p} \qquad \text{[eq. 33]}$$

In this formula $\boldsymbol{\beta}$ stands for a vector of possible regression coefficients, with $\hat{\boldsymbol{\beta}}$ the best fit, and $\mathbf{X}'\mathbf{X}$ is a pxp matrix constructed from the data set. p-1 is the number of independent variables, and n is the number of measurements. $MS_E$ is the mean square error in the dependent variable, evaluated from the quality of the fit to the data. F is the standard F distribution statistic, with $100(1-\alpha)$ the percentage confidence desired. The textbooks I have consulted tend to use this formula for p=2, but do not find it useful for larger values of p, because the hyper-ellipsoid it describes is hard to compute and visualize. Monte Carlo techniques can easily be applied to calculating the shape of this hyper-ellipsoid, however. Consider the hypercube defined by, say, 3 times the individual confidence regions of the various fit parameters. If by Monte Carlo we choose random points in this region, and evaluate inequality 33, we can rapidly develop a group of 1000 (or 10,000) points within the hyper-ellipsoid. These points can be projected onto any plane of our choosing, in order to look for the effects of correlation of pairs of independent variables, for any value of p. (It is more difficult with this technique to see the effects of correlations which involve more than 2 variables, such as $\alpha V_1 + \beta V_2 \approx V_3$.) Figure 2 shows the 90% joint confidence region for the PDX rotation data, as well as the individual confidence regions. Clearly the choice $\alpha = 1$, $\beta = 0$ is exluded by the joint confidence region. On the other hand, while the choice $\alpha = 1$, $\beta = -1$ is included in the 90% confidence region, this figure makes clear that the choice $\alpha = 0.5$, $\beta = 0$, for example, which gives quite a different sense of the physics, is about equally well supported by this particular data.

Figures of this sort are easy to make, both in terms of programming effort and in terms of computer run time. After the 1000 (or 10,000) points

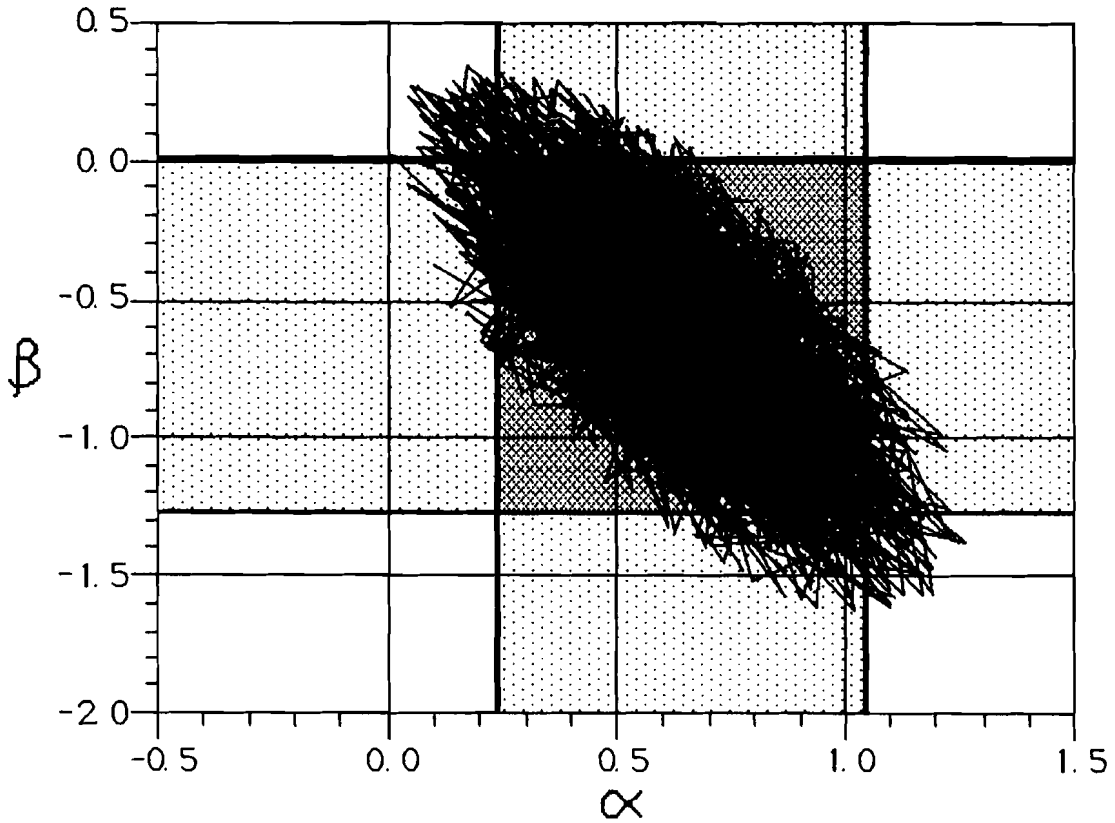


**Figure 2**. 90% individual confidence regions for $\alpha$ (fit coefficient for $P_{abs}$) and $\beta$ (fit coefficient for $\bar{n}_e$), their overlap region, and 90% joint confidence region for $\alpha$ and $\beta$, displayed via Monte Carlo, using 1000 points.

defining the hyper-ellipsoid are stored in memory, they can easily be plotted or examined in any way desired. Interestingly, all the data necessary to communicate the dimensions of this hyper-ellipsoid are contained in the pxp matrix $\mathbf{X'X}$, $\hat{\boldsymbol{\beta}}$, and the values of $MS_E$, p, and n. Plasma physics research frequently comes up against correlated independent variables, so that examination of joint confidence regions could be helpful to us, and perhaps even the communication of $\mathbf{X'X}$ along with the individual confidence regions would be useful.

## Acknowledgments

This work supported by U.S. DoE Contract DE-AC02-76-CHO-3073

The author would like to thank Dr. M. C. Zarnstorff for helpful discussions, and the TFTR data analysis group for collaborative efforts on all fronts.

## References


1. R.J. Hawryluk, "An Empirical Approach to Tokamak Transport" in Physics of Plasmas Close to Thermonuclear Conditions (1979 : Varenna) ed. B. Coppi -- EUR 6584 EN, Brussels, Belgium
2. R.J. Goldston, D.C. McCune, H.H. Towner et al., J. Comp. Phys. 43 (1981) 61
3. S.P. Hirschman, J.C. Whitson, Phys. Fluids 26 (1983) 3553
4. W.M. Stacey, Jr., D.J. Sigmar, to be published in Physics of Fluids
5. H.E. Mynick, "Generalized Banana Drift Transport" PPPL-2271, 1985
   A.H. Boozer, Phys. Fluids 24 (1981) 1387
6. R.B. White, M.S. Chance, Phys. Flu. 27, (1984) 2455
7. J.D. Callen, R.J. Colchin, R.H. Fowler et al., in Plasma Physics and Controlled Nuclear Fusion Research - 1974, IAEA Vienna (1975) 645
8. F.L. Hinton, R.W. Harvey, J.A. Robertson, S.K. Wong, "Prompt Neutral Beam Momentum Input to Tokamak Plasmas" GA-A17387, 1984
9. C.S. Chang, R.W. Harvey, Nucl. Fus. 23 (1983) 935
10. M.C. Zarnstorff, R.J. Goldston, to be published
11. H.P. Furth, P.H. Rutherford, Phys. Rev. Lett. 28 (1972) 545
12. J. Hovey, "The LOCUS Database System - Version C.2" PPPL-TM-364 1984
13. K. Brau, Ph.D. Dissertation, Princeton University 1983
14. K. Brau, M. Bitter, R.J. Goldston et al., Nuc. Fus. 23 (1984) 1643
15. D.C. Montgomery, E.A. Peck "Introduction to Linear Regression Analysis" Wiley and Sons, New York (1982) 126